Accepted Manuscript

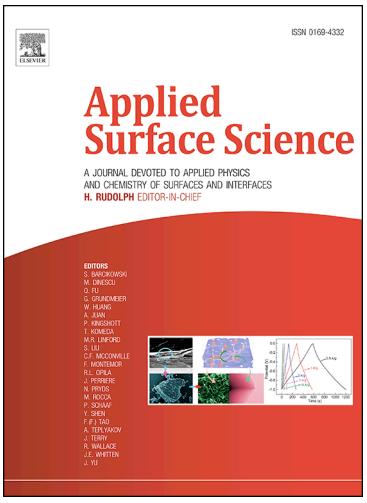

Full Length Article

A Re-assessment of the Isosteric Heat for CCl_4 Adsorption on Graphite

Han Zhang, Shiliang (Johnathan) Tan, D.D. Do, D. Nicholson

PII: S0169-4332(18)32624-2
DOI: https://doi.org/10.1016/j.apsusc.2018.09.198
Reference: APSUSC 40502

To appear in: *Applied Surface Science*

Received Date: 24 July 2018
Revised Date: 21 September 2018
Accepted Date: 24 September 2018

Please cite this article as: H. Zhang, S. (Johnathan) Tan, D.D. Do, D. Nicholson, A Re-assessment of the Isosteric Heat for CCl_4 Adsorption on Graphite, *Applied Surface Science* (2018), doi: https://doi.org/10.1016/j.apsusc.2018.09.198

A Re-assessment of the Isosteric Heat for CCl_4 Adsorption on Graphite

Han Zhang[1,2], Shiliang (Johnathan) Tan[2], D. D. Do[2,*] and D. Nicholson[2]

[1]Key Laboratory of Coalbed Methane Resources and Reservoir Formation Process of
Ministry of Education, China University of Mining and Technology, Xuzhou, Jiangsu, 221006, China

[2] School of Chemical Engineering
University of Queensland, St. Lucia, QLD 4072, Australia

Abstract:

We have carried out molecular simulations of carbon tetrachloride adsorption on graphite, in order to investigate the role of the octopole in potential models for the CCl_4/graphite system, and the temperature dependence of the first-order gas-liquid transition in the first adsorbate layer. Two classes of potential model for carbon tetrachloride were considered: the first has 5 *LJ* sites and the second includes five partial charges to model the leading octopole. Both models are adequate to represent the vapour-liquid equilibrium, suggesting that the octopole makes an insignificant contribution to the properties of the bulk phase. Both models show that adsorbed CCl_4 molecules are delocalized on a graphite surface because of the strong intermolecular interactions. It is found that the *LJ* sites on the chlorine atoms, not the octopole, play the most important role in matching the experimental isotherm and isosteric heat data with simulation. The heat is constant, across the first-order transition of the first adsorbate layer. The simulation results show that both the magnitude of the density jump, and the isosteric heat across the first-order transition, decrease as the temperature increases. This is in qualitative agreement with the 1972 experimental data of Avgul and Kiselev, but these experimental data exhibit an unusually strong decrease in the isosteric heat, and the coexistence region between the two phases displays an unusual asymmetrical shape. Detailed analysis of our simulation results, together with the calculated isosteric heat from the experimental isotherms of Machin and Ross, show that there may be errors associated with the heat data of Avgul and Kiselev at high temperatures.

Keywords: Carbon tetrachloride; graphite; carbon; adsorption; heat of adsorption; simulation

* Corresponding author: d.d.do@uq.edu.au

Highlights:

- Assessment of the heat of adsorption as a function of loading and temperature
- Incommensurate packing of CCl_4 on a graphene surface
- The role of octopole on adsorption is negligible
- Correct choice of the potential model for CCl_4 is important

Graphical abstract:

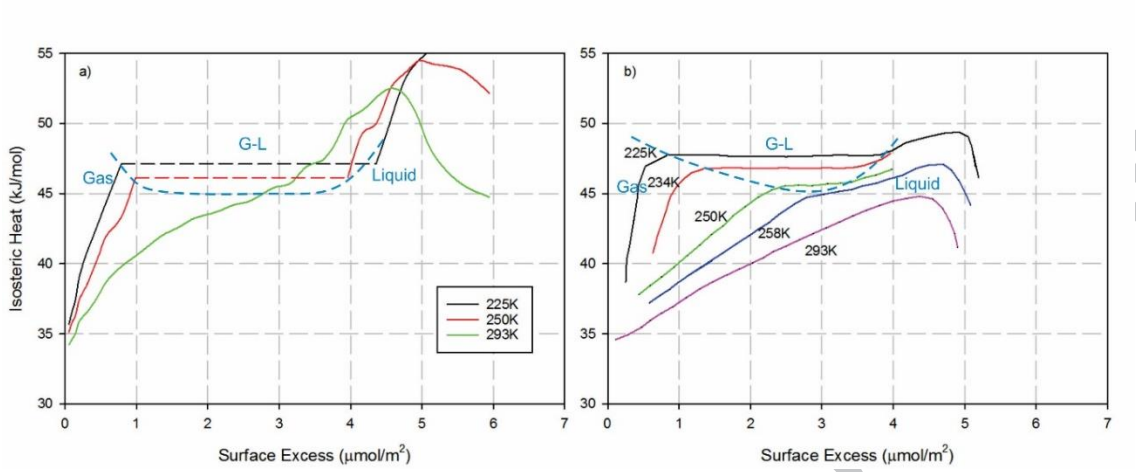

1. Introduction

Carbon tetrachloride (CCl_4) is widely used in industry as a solvent. Since it is harmful to health and to the environment, it is desirable to capture the vapour. A preferred method is by removal by carbonaceous adsorbents because of their low cost relative to other adsorbent materials. The toxicity of carbon tetrachloride incurs a high cost in safety requirements for laboratory experiments; this can be minimized by resort to computer simulation. As a fundamental study, the system attracts interest because of the role played by the tetrahedral structure of the molecule on the microscopic structure of the adsorbate, since the density of the first adsorbate layer is sensitive to molecular orientation. Possibly for the reason mentioned above, experimental studies on adsorption of carbon tetrachloride are limited. Isotherms in the temperature range between 225K and 293K[1] were reported by Pierce [1], and Machin & Ross [2]. The accuracy of these isotherm data was discussed in Do and Do [3]. Isosteric heat data covering the same temperature range were reported by Avgul and Kiselev [4.5]. For the heat curves in the sub-monolayer coverage region at temperatures less than 250K the heat is constant across the gas-liquid first-order transition, in agreement with X-ray data [6]. The constant heat during the 2D-condensation is due to the growth of 2D-adsorbate patches, separated from rarefied regions in the first adsorbate layer [7.8]. As the temperature increases the heat data of Avgul and Kiselev shows that, the region of constant heat shrinks, but that the heat decreases too quickly and the two-phase coexistence region does not have the symmetrical shape exhibited by other adsorbates [9-12]. Although they did not report data for adsorbed density versus pressure, the isotherms reported by Machin and Ross over the same temperature range have been used in the present paper to assess the heat data from the Clausius-Clapeyron equation.

[1] The bulk triple and critical temperatures are 249K and 556K.

2. Simulation details

2.1 Fluid and Solid model

The *X*-ray and neutron diffraction data on the intra- and inter-molecular structure [13-16] give a C-Cl bond length of between 1.77 Å and 1.85 Å, and the closest inter-molecular (C-C) distance is between 6.2 Å and 6.7 Å. These values are used in the development of potential models for carbon tetrachloride. Early potential models which treat CCl_4 as a 1-site molecule [16-19], fail to describe the thermodynamic properties of CCl_4 because the interaction between chlorine atoms is much stronger than that between the carbon atoms, which means that the positions of the four chlorine atoms is important. A more accurate model, must therefore, account for all atoms in the tetrahedral CCl_4 molecule. Previously, 5-site models have been shown to give a good account of the vapour-liquid equilibrium (*VLE*) as well as adsorption of CCl_4 on graphite [20-23]. These potential models have been reviewed in Do and Do [3]. Recently a new model in this class was proposed by Guevara-Carrion *et al*. which includes partial charges to model the leading electrostatic octopole [24]. In bulk liquid or solid CCl_4, most models show that a face-to-face interlocking structure is the most favoured configuration as shown in *Figure* 1a [10.22]. On graphite, Avgul and Kiselev [11.12] discussed three typical configurations: (1) a tripod configuration with three chlorine atoms facing the surface, (2) an edge-down configuration with two Cl atoms facing the surface, and (3) an inverted tripod configuration. The monolayer density depends on the orientation of the molecules; for example, a first adsorbate layer comprised of only the energetically favourable tripod configuration gives the lowest monolayer density. Combination of the configurations detailed above at finite temperatures is possible because of the balance between the energy and the entropy to minimize the free energy [25].

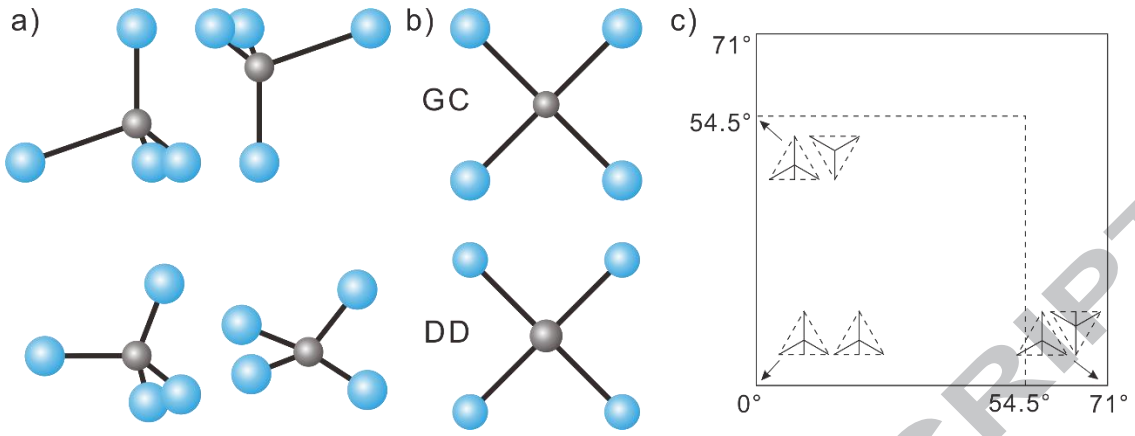

Figure 1 Illustration of the favoured pairwise configurations of tetrahedral molecules; (a) face-to-face and face-to-edge configurations, (b) the geometrical structure of the molecular *GC* [24] and *DD* [3] models, and (c) possible configurations of the assembly of 2 molecules on a surface.

In this simulation study, we have focussed on two potential models: (1) the 5-site (*LJ*) model proposed by Do and Do (*DD*) [3], (2) the 10-site (5*LJ*+5*q*) model of Guevara-Carrion *et al.* (*GC*) [30]. The molecular parameters for these models are listed in Table 1.

It is to be noted that although the *GC* model has a larger separation between the dispersive site on the carbon atom and the other dispersive sites, the overall molecular size conforms to the experimental data because collision diameters used are smaller than those of the *DD* model (*Figure* 1b).

Table 1 Molecular parameters for the various CCl_4 potential models

Model	Atom	Collision Diameter (nm)	Reduce Well Depth (K)	Bond Length (nm)	Charge	Reference
DD	C	0.46	39	0.1766	-	[3]
	Cl	0.35	105			
GC	C	0.281	12.37	0.2044	-0.362	[24]
	Cl	0.325	212.6		0.0905	

Depending on the size and shape of the adsorbate molecules, the first adsorbate layer may form a packing that is commensurate with the graphite lattice; for symmetrical tetrahedral adsorbates, the possible lattice for an adsorbate in a hexagonal centred packing (HCP) are $\sqrt{3}a_{Gr}$, $2a_{Gr}$, $\sqrt{7}a_{Gr}$, $3a_{Gr}$, *etc.*, where $a_{Gr} = 0.246nm$ is the graphite lattice constant. For instance, methane forms a $\sqrt{3}\times\sqrt{3}a_{Gr}$ packing [26-28], CF_4 forms a $2\times 2a_{Gr}$ packing [29.30], and CCl_4 with a size between $\sqrt{7}a_{Gr}$ and $3a_{Gr}$, the monolayer density is 3.96 μmol/m^2 if it adopts a $\sqrt{7}a_{Gr}$ commensurate packing (Table 2).

Table 2 Lattice constants and the adsorbate commensurate density

Packing	Lattice constant (nm)	Surface density (μmol/m^2)
$\sqrt{3}a_{Gr}$	0.426	10.54
$2a_{Gr}$	0.492	7.92
$\sqrt{7}a_{Gr}$	0.651	3.96

We used two models for graphite. The first model treats graphite as a continuum solid with an energetically homogeneous surface; the potential energy of interaction with an *LJ* site is given by the 10-4-3 equation (*eq*. 1) with the molecular parameters derived by Steele [31].

$$\varphi_{sf} = 2\pi\left(\rho\sigma_{sf}^2\right)\varepsilon_{sf}\left[\frac{2}{5}\left(\frac{\sigma_{sf}}{z}\right)^{10} - \left(\frac{\sigma_{sf}}{z}\right)^{4} - \frac{1}{3}\frac{\sigma_{sf}^4}{\Delta(z+0.61\Delta)^3}\right] \quad (1)$$

The second is the Corrugation and Anisotropy (CA) model that accounts for the hexagonal arrangement of carbon atoms and the anisotropy of polarizability of graphite [32]. Details of this model are given in references [33, 34].

2.2 Simulation Details

Simulations were carried out using the kinetic Monte Carlo (*k*MC) method in the canonical and grand canonical ensembles [35-37]. *k*MC provides a very efficient method for the calculation of chemical potential. Instead of using the ensemble average, as in Metropolis Monte Carlo, the *k*MC scheme assigns a time of existence for each configuration, defined as the inverse of the sum of molecular mobilities, *R*:

$$\tau = \frac{\ln(1/\xi)}{R} = \frac{\ln(1/\xi)}{\sum_j \exp(u_j / k_B T)} \tag{2}$$

where ξ is a random number, introduced to maintain a stochastic sampling in the *kMC* simulation, and u_j is the potential energy of interaction molecule "*i*" with all entities in the system. The isosteric heat in the grand canonical simulations was obtained from number and energy fluctuations:

$$q_{st} = k_B T - \frac{f\langle U, N\rangle}{f\langle N, N\rangle} \tag{3}$$

where $f\langle X, Y\rangle = \langle XY\rangle - \langle X\rangle\langle Y\rangle$. To obtain the isosteric heat across the first order transition, we used the simulation results in a canonical ensemble, with:

$$q_{st} = k_B T - \frac{\partial\langle U\rangle}{\partial N} \tag{4}$$

We used at least 1×10^9 configurations in both the equilibration and sampling stages.

The experimental isosteric heat was found from isotherms measured at different temperatures, using the Clausius-Clapeyron equation, which assumes that the adsorptive vapour is an ideal gas and that the molar volume of the gas phase is very much larger than that of the adsorbate phase:

$$q_{st} = \frac{RT_1T_2}{T_2 - T_1} \ln\left(\frac{P_2}{P_1}\right) \tag{5}$$

The orientation angle of a molecule is defined as the angle between a normal vector from the graphite surface and a reference vector pointing from the carbon atom to the chlorine atom that is furthest from the surface [38]. The upper limit of this angle is 71°, corresponding to the inverted tripod configuration. The orientation distribution is defined as follows

$$\theta_z = \frac{< N_i >}{\sin(\alpha) \times \Delta\alpha} / < N > \tag{6}$$

where $\langle N_i \rangle$ is ensemble average number of molecules whose angles fall between α and α+Δα, and $\langle N \rangle$ is the total number of particle in the system. Δα was set as 1° in these calculations.

The orientation between a pair of molecules in the adsorbed phase affects the density of the first adsorbate layer. The orientation angles between any two molecules with centres of mass separated by less than 0.8nm were monitored and noted as being an "assembly pair". For example, for a pair of molecules having a tripod configuration and an edge-down configuration (2 Cl atoms facing the surface), the angles are (0°, 54.5°). We define the ensemble average number of molecules that falls into an assembly pair with the angles α and β as:

$$\langle N(\alpha, \beta) \rangle = \left\langle \sum_{i=1}^{N} \sum_{j>i}^{N} N_i \, \delta(i, j) \right\rangle \tag{7a}$$

where

$$\delta(i, j) = \begin{cases} 1 & \text{if } d_{i,j} < 0.8nm \\ 0 & \text{otherwise} \end{cases} \tag{7b}$$

This pair distribution, presented on a contour plot, indicates how the pairs interlock with each other as shown in *Figure* 1c. The linear dimensions of the graphite surface are 9.84×8.52nm^2.

3. Results and discussion

3.1 The Effect of the Graphite Model

A good potential model for the description of adsorption is one that correctly describes the vapour liquid equilibrium (*VLE*). The *DD* and *GC* models for CCl_4, chosen in this paper, both satisfy this criterion (Figure S1). Both models have a gas-liquid (*G*-*L*) transition at temperatures lower than 260K which is identified as the critical temperature of first adsorbate layer, as shown by the transition in the grand canonical isotherms and the *S*-shaped curve of the canonical isotherms in *Figure* 2. We particularly note that the loop through the coexistence region between the gas and liquid states (shown as a dashed line) is symmetrical, as is also observed for many other adsorbates.

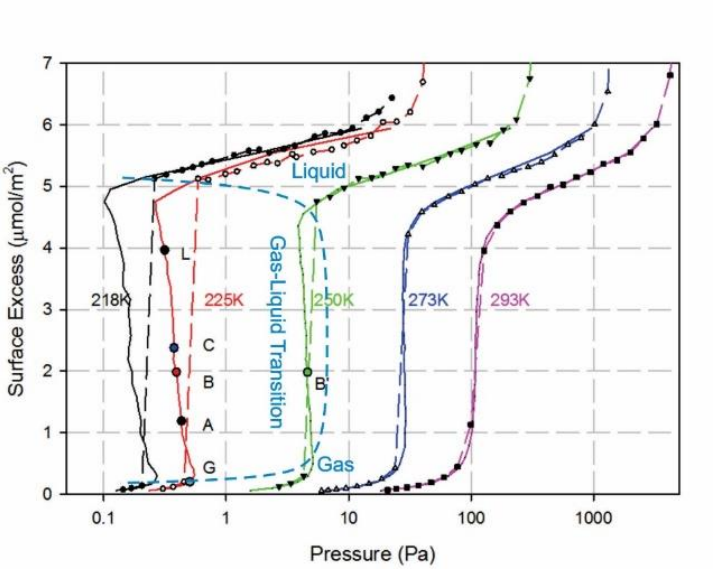

Figure 2 Isotherms simulated with the grand canonical (dashed lines) and canonical (solid lines) ensembles using the *GC* model. The isotherms simulated with the *DD* model are shown in Figure S2.

Pierce [1] reported experimental isotherms at 232K, 248K, 253K and 273K, but we note that, unlike our simulation results and the isosteric heat data of Avgul and Kiselev [4.5] that show a first-order transition at temperatures less than 260K, Pierce's isotherms do not show any clear transition. We attribute this to the energetic heterogeneity of the carbon used by Pierce.

Figure 3 shows the simulated isotherms for the different models for carbon tetrachloride and graphite. Since there is no reliable experimental isotherm data, it is not possible to judge which model is the better representation for the CCl_4/Gr system. Neither the *GC* nor the *DD* model show commensurate packing of the CCl_4 molecules, but the *GC* model performs better in the describing of isosteric heat (*Figure* 4a). Hereafter we focus on the *GC* model and the homogeneous graphite.

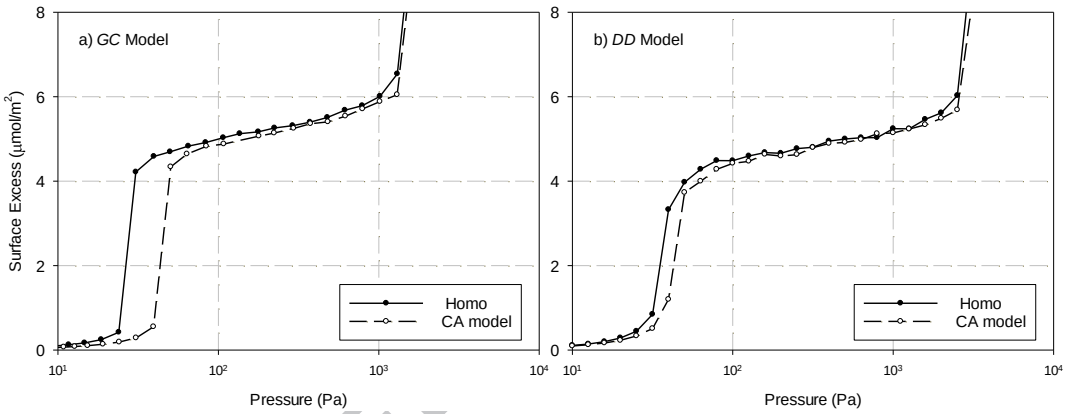

Figure 3 Comparison between the simulated isotherms with different adsorbent and adsorbate models at 273K, (a) the *GC*-model, (b) the *DD* model

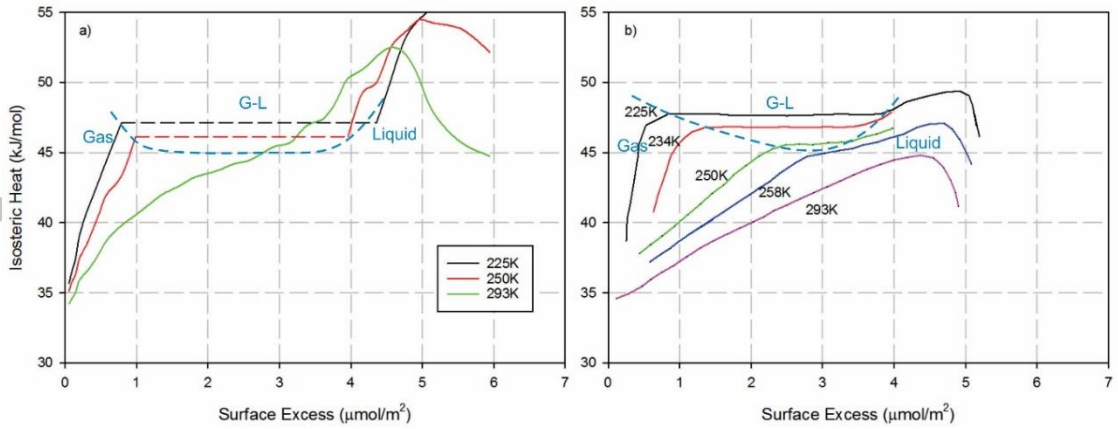

Figure 4 Isosteric heat versus loading (a) simulated with the *GC* model; (b) experimental isosteric heat from Avgul and Kiselev [4]. The gas-liquid coexistence envelope is shown as a dashed line. Results for the *DD* model are given in Figure S3.

The experimental isosteric heat data from Avgul and Kiselev [4] are shown in *Figure* 4b. The results from simulations with the *GC* model, shown in *Figure* 4a, are in better agreement with experiment than simulations with the *DD* model (see Figure S3) which does not reproduce the constant isosteric heat through the gas liquid transition region at sub critical temperatures. The simulated isosteric heat decreases with temperature, which is in qualitative agreement with experiment but the experimental data decreases more steeply, and the loop in the coexistence region has a very unusual asymmetrical shape (*Figure* 4b) compared to the symmetrical shape found in both experiment and simulation for other adsorbates, including the phase diagram derived from the experimental *XRD* data for CCl_4 [6]. Possible errors associated with the experimental data of Avgul and Kiselev are discussed in *Section* 3.3.

3.2 Local properties

3.2.1 Local density and radial density distributions

The 2D maps of the local density distribution (*2D-LDD*) in *Figure* 5 show the evolution of the adsorbed density with temperature. At temperatures below the triple point (250K) there is coexistence between a 2D-adsorbed phase and the rarefied phase on the surface. As molecules are added to the system they adsorb at the boundary line separating these two phases. The adsorbed phase first grows into a circular island (*Figure* 5a), then, as more molecules are added to the adsorbed phase, the island changes shape to a strip and expands (*Figure* 5b-c).

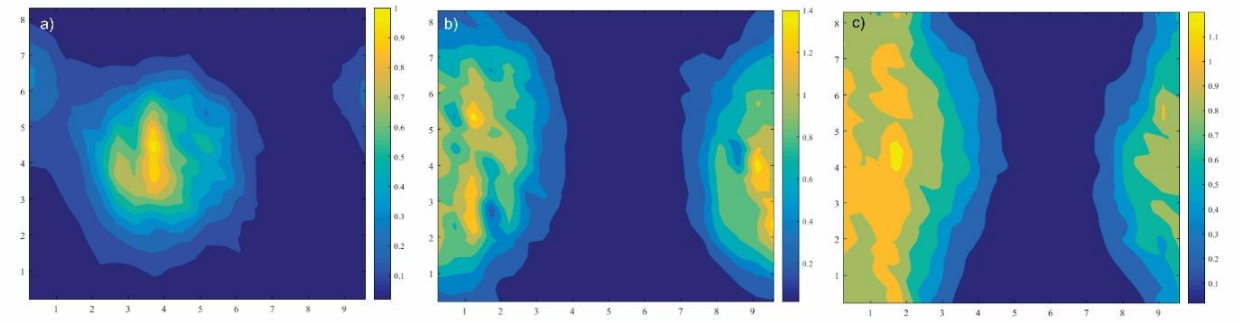

Figure 5 Plots of the 2D local density for different loadings within the *G-L* transition at 225K (a, b and c, correspond to Points A, B and C marked in Figure 3).

The density of the 2D-adsorbed phase across the transition is lower at higher temperatures, and the interface separating the adsorbed phase and the rarefied phase becomes more diffuse due to thermal fluctuations, as shown in *Figure* 6 Comparison between the 2D local density at 225K (a) and 250K(b) for points B and B' (with the same loading at 2μmol/m2)at temperatures of 225K and 250K for points at the same loading (2μmol/m^2).

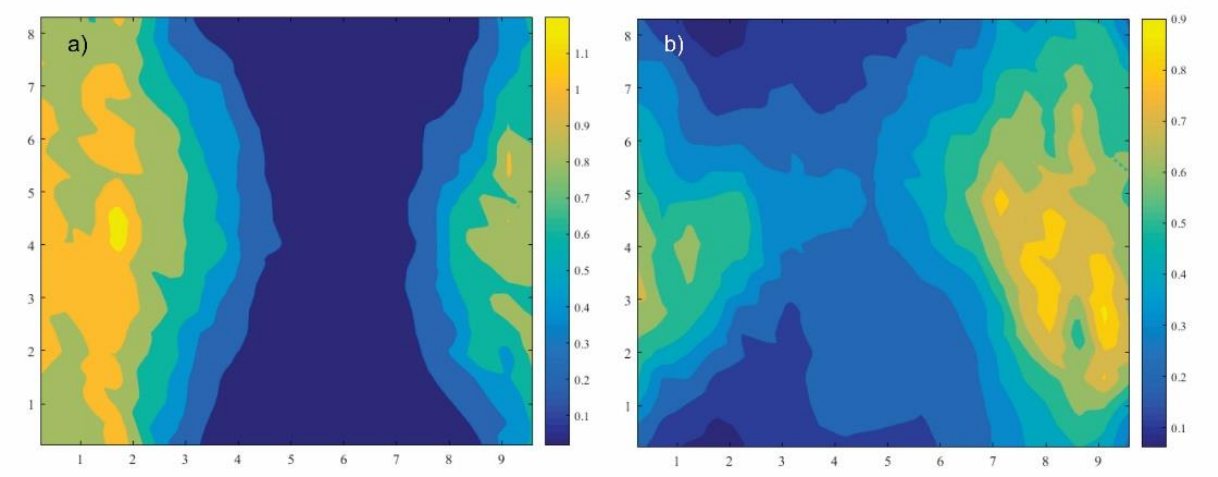

Figure 6 Comparison between the 2D local density at 225K (a) and 250K(b) for points B and B' (with the same loading at 2μmol/m^2)

The *RDD* for molecules in the first layer, shown in *Figure* 7, supports the *2D-LDD* discussed above. The positions of the peaks give the most probable distances between neighbouring molecules. The area under the first peak at the same loading decreases significantly and the separation distance between nearest molecules increases with temperature (*Figure* 7a). The ratio of the separation at the second peak to that at the first is around 1.85, which is close to the theoretical value of $\sqrt{3}$ for *HCP* packing, indicating that the layer adopts an *HCP* packing.

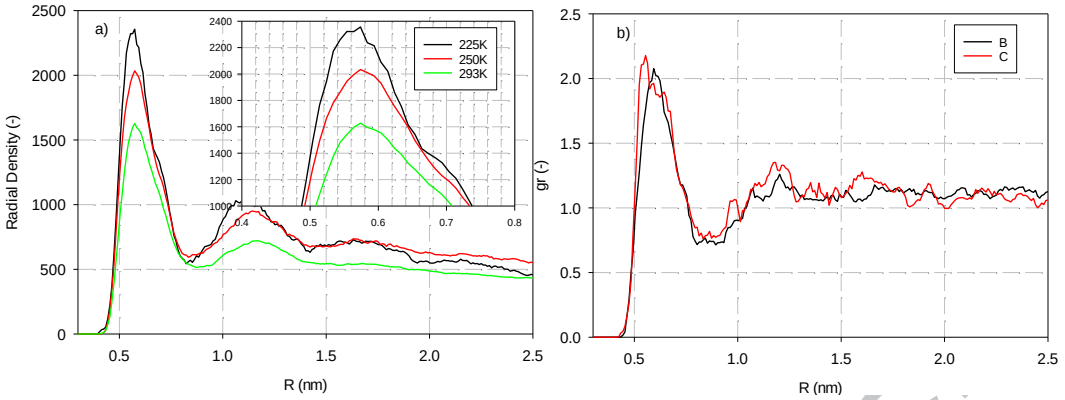

Figure 7 (a) Plots of the radial density distribution at Point B marked in Figure 3 simulated with the *GC* model for different temperatures (the *DD* model shows the same trends); (b) the radial density distribution along the phase boundary at various loadings for 225K.

The *2D-LDD* for the adsorbed phase in *Figure* 5 shows that across the *G-L* transition, new molecules adsorb along the boundary separating the two phases. To better quantify the constant heat across the transition, we investigate whether this is due to constant contributions from the solid-fluid (*SF*) interactions and the fluid-fluid (*FF*) interactions, or to compensation between the decrease in the *SF* interactions and the increase in *FF* interactions. To resolve this question, we isolated the molecules in the interfacial region separating the two phases, and determined the radial density distribution of this sub-population. The first adsorbate layer was divided into 2D-bins of size 1.6×1.6 nm^2 (1.6nm is twice the separation at the minimum between the first and second peak in the *RDD*), which can accommodate 3-4 molecules in the liquid state. Thus, a molecule is defined as being on the phase boundary when a bin contains only one molecule. The density in the rarefied phase is too low to affect the result, therefore the *RDD* of this sub-population shows the number of nearest neighbours along the boundary separating the two phases. Points B and C are selected (marked in *Figure* 3), and the results indicate that molecules along the phase boundary interacting with 3.7 nearest neighbours, from integrations

of the *RDD* of the sub-population in *Figure* 7b; resulting in a constant contribution to the isosteric heat from the *FF* interactions.

3.2.2 Orientation Density Distribution

The orientation density distributions (*ODD*) of both the *DD* and *GC* models at low loadings show that most molecules prefer the energetically favourable tripod configuration but other configurations are possible as the temperature is increased (*Figure* 8). However, the *ODD* of the *DD* model shown in *Figure* 9 indicates a stronger preference for the tripod configuration.

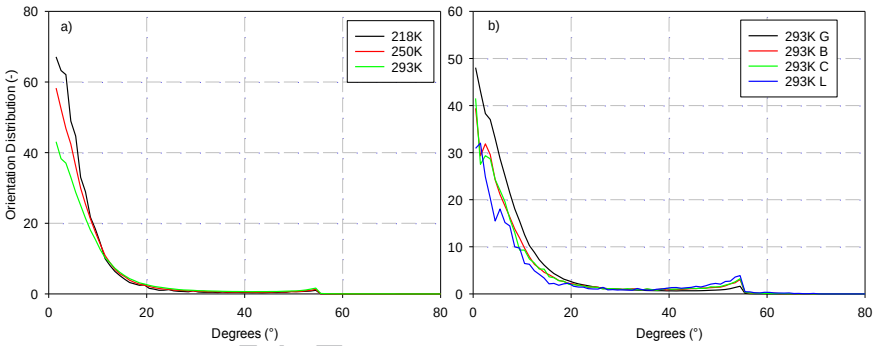

Figure 8 (a) The orientation density distributions (*ODD*) for loading at Point G (0.4 μmol/m^2, marked in *Figure* 3) at different temperatures, simulated with the *GC* model; (b) The *ODD*s at various loadings (marked in *Figure* 3) at 293K with the *GC* model.

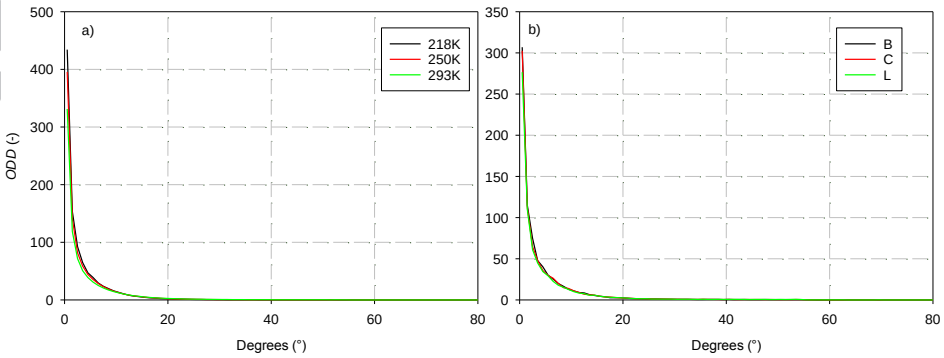

Figure 9: (a) The *ODD*s for loading at Point G with the *DD* model for different temperatures; (b) *ODD* across the *G-L* transition with the *DD* model at 293K, at loadings as marked in *Figure* 3.

The most favoured configuration between a pair of molecules in the bulk is the face-to-face configuration (0°, 71°). To investigate how a pair of molecules arrange in the presence of a surface, we considered the pairwise orientation assembly (*eq*. 7). The *GC* and *DD* models have completely different pair assembly of orientations, as shown in *Figure* 10.

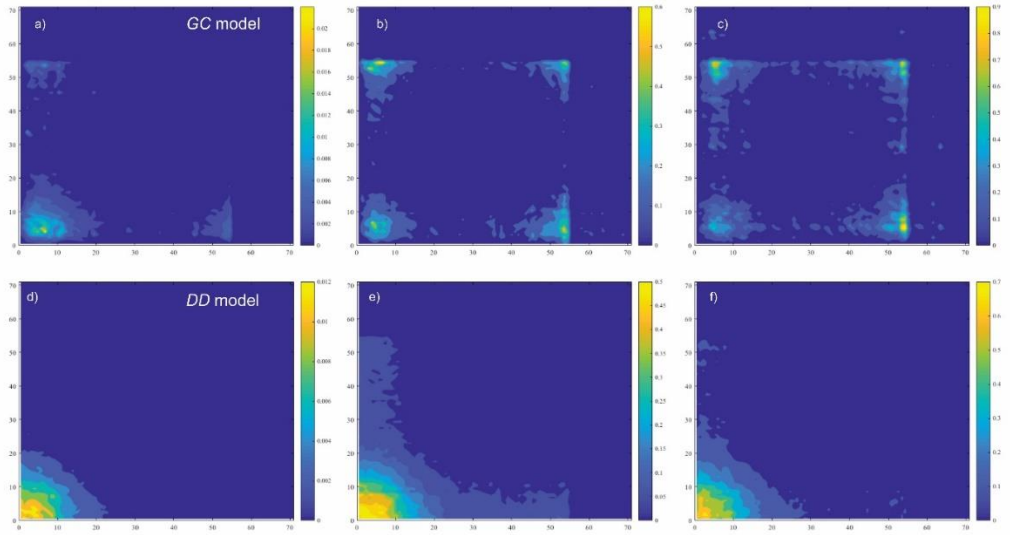

Figure 10 The pair orientation distribution at 225K at loadings of G, B and C (marked in Figure 3) for the *GC* model (a-c) and the *DD* model (d-f).

At low loadings, both models show the tripod configuration as expected, but as the loading is increased, other configurations begin to appear in simulations with the GC model, in addition to the tripod/tripod pairwise configuration, which increases the entropy of the system. On the other hand, the *DD* model continues to favour the tripod/tripod configuration (*Figure* 10). This can be attributed to the larger collision diameter of the chlorine atom in the *DD* model, compared to that in the *GC* model (*Figure* 1c). This makes the surface of the GC model of CCl_4 more corrugated, enabling molecules to interlock better when there is a combination of tripod configurations and other configurations. Therefore, in the *GC* model, the *FF* interactions that compensate for the decrease in the *SF* interactions are enhanced. Further experiments are required to resolve the structure of CCl_4 molecules as a function of loading.

3.3 Heat evolution with temperature

Avgul and Kiselev [4] reported a significant decrease in the experimental isosteric heat across the *G-L* transition as the temperature is increased. Although the simulated isosteric heat derived from the *GC* model captures this decrease better than the *DD* model (Figure S3), it still does not accord with the significant decrease displayed in experiments.

At 225K (*Figure* 12), the isosteric heat increases linearly at low loadings, and across the *G-L* transition, the heat is constant as explained earlier. Beyond the transition the isosteric heat increases again because of the densification of the first adsorbate layer. To gain a better insight into the adsorption mechanism we decomposed the isosteric heat into the contributions from the *SF* and *FF* interactions. The isosteric heat at zero loading at 225K is 35kJ/mol, which is solely from the *SF* interaction; this agrees with the minimum in the *SF* potential energy (Figure S4). This value corresponds to a tripod configuration at zero loading. As the loading is increased, the contribution from the *SF* interactions shows a modest decrease, indicating the appearance of configurations other than the tripod configuration, while the contribution from *FF* interactions increases linearly because of the increase in the number of neighbouring molecules. Across the *G-L* transition, the contributions from both the *SF* and *FF* interactions remains essentially constant, as explained earlier.

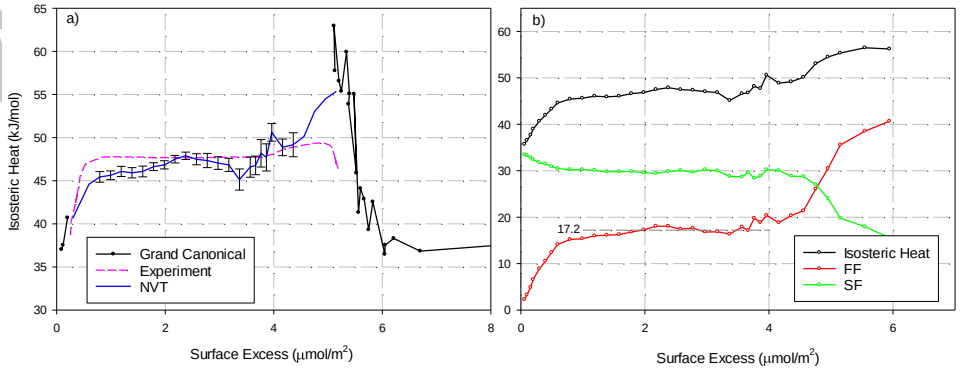

Figure 11 Plots of the simulated isosteric heat versus loading at 225K, obtained with the GC model from simulations in the canonical and grand canonical ensembles. The error bars are associated with the canonical results; (b) the contributions of the *SF* and *FF* interactions to the canonical isosteric heat

When the temperature is increased, there is a small decrease in the isosteric heat at zero loading due to the increase in the number of the configurations other than the tripod configuration, as discussed in *Section* 3.2.

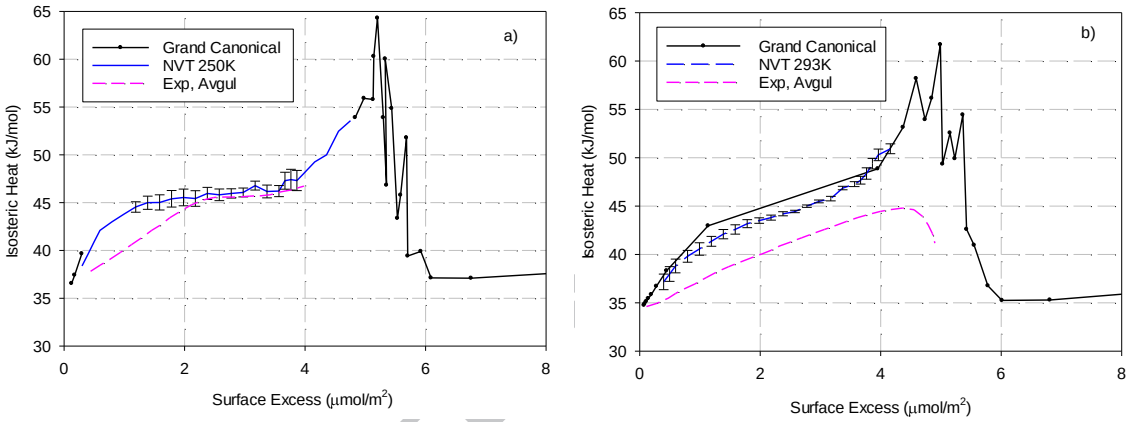

Figure 12 Plots of the canonical and grand canonical simulated isosteric heat versus loading with the *GC* model: (a) 250K and (b) 293K. Experimental results are shown as red dashed lines.

The major difference between the *DD* model and the *GC* model comes from the different molecular parameters and the positions of *LJ* sites (see Table 1), although statistically these models are equivalent as seen in the *VLE* results and the *SF* profiles (Figure S1 and S4). The role of the electrostatic interactions from the octopole is insignificant as shown in *Figure* 13a, where it is seen that there is no difference between the isosteric heats from simulations with or without partial charges. The contribution from the partial charges is less than 0.6% of the total *FF* interaction. The 2D distribution of the orientation of the pair assembly shown in *Figure* 13b (which is similar to *Figure* 10) confirms this conclusion.

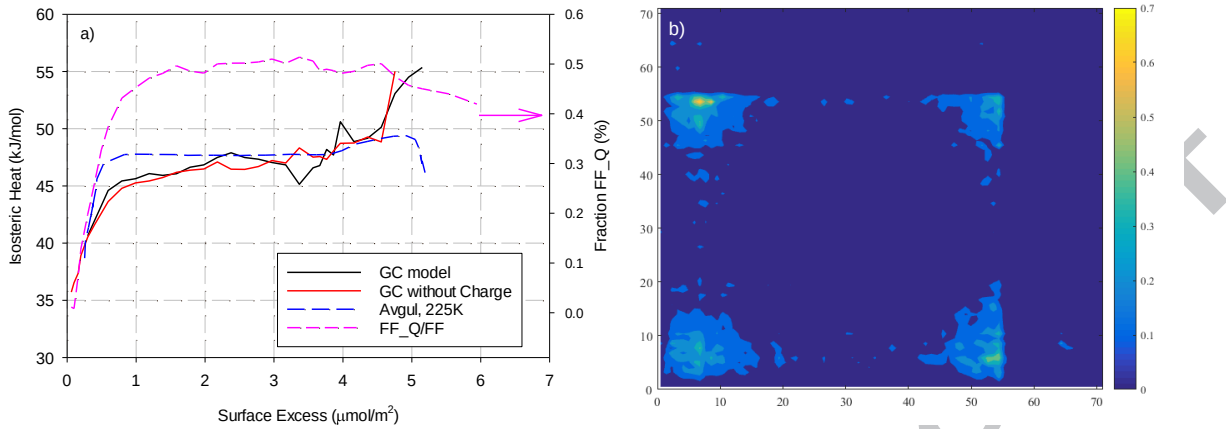

Figure 13 (a) Simulation results for the *GC* model, with and without partial charges, and the contribution of electrostatic (FF_Q) term; (b) the orientation of the pair assembly at loading B (marked in Figure 3).

The differences between our simulation results and the experiment data of Avgul and Kiselev [4] are as follows: (1) The experiments show a bigger 2D gas density before the *G-L* transition, which leads to a lower increase of the heat versus density at low loadings. (2) The heat released during and beyond the *G-L* transition at higher temperatures is much lower than in the simulation results (*Figure* 12b). As seen in *Figure* 4, the co-existence region derived from the simulated isosteric heats versus loading show the same symmetrical loop as the isotherms, while the heat data of Avgul and Kiselev shows a highly asymmetric shape and a much higher 2D gas density before the transition. We resolve this discrepancy in *Figure* 14, by plotting the isosteric heats from the simulations, the experiments from Avgul and Kiselev and the calculated isosteric heats from the isotherms of Machin and Ross [2] at low loadings. Furthermore, the isosteric heat reaches a maximum of *45kJ/mol* experimentally on completion of the first adsorbate layer, and *60kJ/mol* in simulation. This maximum heat can be estimated theoretically as the sum of the heat at zero loading (*35kJ/mol*) and the simulated heat released by the *FF* interaction with six neighbouring molecules of *25kJ/mol*. The contribution from interaction with one neighbour is therefore *4kJ/mol*, in agreement with the average energy of a

pair of CCl_4 molecules (Figure S4). This analysis, casts doubt on the accuracy of the experimental isosteric heat of Avgul and Kiselev at high temperatures.

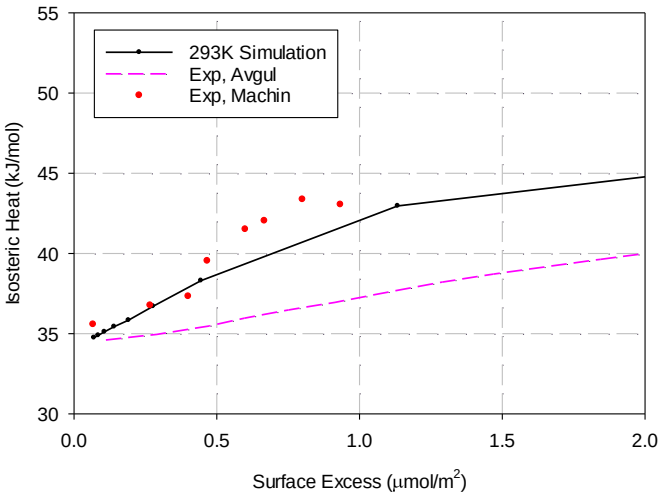

Figure 14 Comparison between simulation, the experiment of Avgul & Kiselev, and the calculated isosteric heat obtained by applying the Clausius-Clapeyron equation (eq. 5) to the experimental isotherm data of Machin and Ross.

Supporting Information

The additional results that supports the discussion include: (1) Vapor and liquid equilibrium diagram for CCl_4 models included, (2) isotherms, and (3) isosteric heat of *DD* model, (4) solid-fluid profile along *Z* direction and fluid-fluid profile for *GC* and *DD* model.

Acknowledgement: This project is funded by the Australian Research Council (DP16013540) and the Fundamental Research Funds for the Central Universities (No.2017CXNL03)

References

References:

[1] C. Pierce, Hill equation for adsorption on uniform surfaces, J. Phys. Chem. 72(1968) 1955-1959.

[2] W.D. Machin, S. Ross, On physical adsorption .17. Experimental verification of 2-dimensional Van der Waals equation of state above and below critical temperature, Proceedings of the Royal Society of London Series a-Mathematical and Physical Sciences, 265(1962) 455.

[3] D.D. Do, H.D. Do, Adsorption of Carbon Tetrachloride on Graphitized Thermal Carbon Black and in Slit Graphitic Pores: Five-Site versus One-Site Potential Models, The Journal of Physical Chemistry B, 110(2006) 9520-9528.

[4] N.N. Avgul, A.V. Kiselev, Physical adsorption of gases and vapors on graphitized carbon black, Marcel Dekker INC, New York, 1970.

[5] G.I. Berezin, A.V. Kiselev, R.T. Sagately, M. Serdobov, Heat of adsorption of carbon tetrachloride on a graphitised carbon black above and below 2-dimensional critical temperature, Russian Journal of Physical Chemistry, USSR, 1(1969) 118.

[6] P.W. Stephens, M.F. Huth, Adsorption of CCl4 on graphite, Phys. Rev. B, 32(1985) 1661-1672.

[7] V.T. Nguyen, D.D. Do, D. Nicholson, On the Heat of Adsorption at Layering Transitions in Adsorption of Noble Gases and Nitrogen on Graphite, J. Phys. Chem. C, 114(2010) 22171-22180.

[8] D.D. Do, D. Nicholson, H.D. Do, On the anatomy of the adsorption heat versus loading as a function of temperature and adsorbate for a graphitic surface, J. Colloid Interf. Sci., 325(2008) 7-22.

[9] A. Thomy, X. Duval, Stepwise isotherms and phase-transitions in physisorbed films, Surf. Sci., 299(1994) 415-425.

[10] A.H. Li, S. Huang, S.D. Chao, Molecular dynamics simulation of liquid carbon tetrachloride using ab-initio force field, The Journal of Chemical Physics, 132(2010) 24506.

[11] N.N. Avgul, A.V. Kiselev, I.A. Lygina, Potential energy of adsorption of the sphere-like molecules CH4, C(CH3) 4 and CCl4 on graphite, Bulletin of the Academy of Sciences of the USSR, Division of chemical science, 8(1962) 1264-1270.

[12] N.N. Avgul, A.V. Kiselev, I.A. Lygina, Isotherms and heats of adsorption of sphere-like molecules on graphitized carbon black - potential energies and chances in thermodynamic functions upon adsorption on graphite, Transactions of the Faraday Society, 59(1962) 2113.

[13] R.W. Gruebel, G.T. Clayton, Determination of Electron and Molecular Radial Distribution Functions for Liquid Carbon Tetrachloride by X - Ray Diffraction, The Journal of Chemical Physics, 46(1967) 639-643.

[14] D.E. O'Reilly, E.M. Peterson, C.E. Scheie, Molecular rotation in liquid and solid carbon tetrachloride, The Journal of Chemical Physics, 60(1974) 1603-1606.

[15] P.A. Egelstaff, D.I. Page, J.G. Powles, Orientational correlations in molecular liquids by neutron scattering - carbon tetrachloride and germanium tetrabromide, Mol. Phys., 20(1971) 881.

[16] A.H. Narten, M.D. Danford, H.A. Levy, Structure and Intermolecular Potential of Liquid Carbon Tetrachloride Derived from X - Ray Diffraction Data, The Journal of Chemical Physics, 46(1967) 4875-4880.

[17] J.O. Hirschfelder, C.F. Curtiss, R.B. Bird, Molecular Theory of Gases and Liquids, 2nd ed, J. Wiley and Sons, New York, 1964.

[18] R. Radhakrishnan, K.E. Gubbins, M. Sliwinska-Bartkowiak, Global phase diagrams for freezing in porous media, The Journal of Chemical Physics, 116(2002) 1147-1155.

[19] T. Suzuki, T. Iiyama, K.E. Gubbins, K. Kaneko, Quasi-Symmetry Structure of CCl4 Molecular Assemblies in a Graphitic Nanopore: A Grand Canonical Monte Carlo Simulation, Langmuir, 15(1999) 5870-5875.

[20] F.S. Adan, A. Banon, J. Santamaria, Monte-Carlo calculations for liquid carbon-tetrachloride, Chem. Phys. Lett., 107(1984) 475-480.

[21] I.R. McDonald, D.G. Bounds, M.L. Klein, Molecular dynamics calculations for the liquid and cubic plastic crystal phases of carbon tetrachloride, Mol. Phys., 45(1982) 521-542.

[22] T.M. Chang, K.A. Peterson, L.X. Dang, Molecular-dynamics simulations of liquid, interface, and ionic solvation of polarizable carbon-tetrachloride, J. Chem. Phys., 103(1995) 7502-7513.

[23] L.J. Lowden, D. Chandler, Theory of intermolecular pair correlations for molecular liquids. Applications to the liquids carbon tetrachloride, carbon disulfide, carbon diselenide, and benzene, The Journal of Chemical Physics, 61(1974) 5228-5241.

[24] G. Guevara-Carrion, T. Janzen, Y.M. Munoz-Munoz, J. Vrabec, Mutual diffusion of binary liquid mixtures containing methanol, ethanol, acetone, benzene, cyclohexane, toluene, and carbon tetrachloride, J. CHEM. PHYS., 144(2016).

[25] M. Marzec, B. Kuchta, L. Firlej, Adsorption and phase transitions in adsorbed systems: structural properties

of CCl4 layers adsorbed on a graphite surface, J. Mol. Model., 13(2007) 537-542.
[26] J.M. Phillips, Methane adsorbed on graphite. II. A model of the commensurate-incommensurate transitions, Phys. Rev. B, 29(1984) 5865-5871.
[27] H.Y. Kim, W.A. Steele, Computer-simulation study of the phase-diagram of the CH4 monolayer on graphite - corrugation effects, Phys. Rev. B, 45(1992) 6226-6233.
[28] S. Jiang, K.E. Gubbins, J.A. Zollweg, Adsorption, isosteric heat and commensurate-incommensurate transition of methane on graphite, Mol. Phys., 80(1993) 103-116.
[29] K. Kjær, M. Nielsen, J. Bohr, H.J. Lauter, J.P. McTague, Monolayers of CF4 adsorbed on graphite, studied by synchrotron x-ray diffraction, Phys. Rev. B, 9(1982) 5168.
[30] Q.M. Zhang, H.K. Kim, M. Chan, Phase-diagram and phase-transitions of monolayer and bilayer CF4 on graphite, Phys. Rev. B, 34(1986) 8050-8063.
[31] W.A. Steele, Physical interaction of gases with crystalline solids .1. gas-solid energies and properties of isolated adsorbed atoms, Surf. Sci., 36(1973) 317-352.
[32] W.E. Carlos, M.W. Cole, Anisotropic He-C pair interaction for a He atom near a graphite surface, Phys. Rev. Lett., 43(1979) 697-700.
[33] Y. Zeng, K. Horio, T. Horikawa, K. Nakai, D.D. Do, D. Nicholson, On the evolution of the heat spike in the isosteric heat versus loading for argon adsorption on graphite-A new molecular model for graphite & reconciliation between experiment and computer simulation, Carbon, 122(2017) 622-634.
[34] L. Prasetyo, S.J. Tan, Y. Zeng, D.D. Do, D. Nicholson, An improved model for N2 adsorption on graphitic adsorbents and graphitized thermal carbon black—The importance of the anisotropy of graphene, The Journal of Chemical Physics, 146(2017) 146.
[35] A.F. Voter, Introduction to the kinetic Monte Carlo method, Springer Netherlands, Dordrecht, 2007.
[36] C.C. Battaile, The Kinetic Monte Carlo method: Foundation, implementation, and application, Comput. Method. Appl. M., 41(2008) 3386-3398.
[37] A.P.J. Jasen, Kinetic Monte Carlo Algorithms, Springer, Berlin, Heidelberg, 2012.
[38] B. Dunweg, U.D. Schiller, A.J. Ladd, Statistical mechanics of the fluctuating lattice Boltzmann equation, Phys. Rev. E 76(2007) 36704.

Graphical abstract

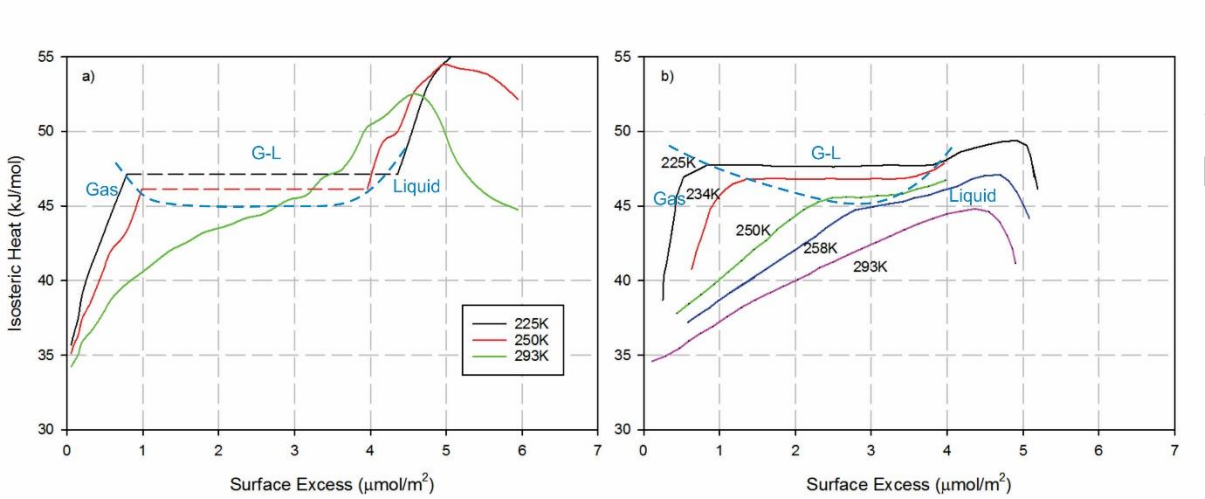

Highlights:

- Assessment of the heat of adsorption as a function of loading and temperature
- Incommensurate packing of CCl4 on a graphene surface
- The role of octopole on adsorption is negligible
- Correct choice of the potential model for CCl4 is important